2018

Enhanced UV-light detection based on ZnO nanowires/graphene oxide hybrid using cost-effective low temperature hydrothermal process

Tariq AlZoubi
University of the Middle East

Hamzeh Qutaish
University of Wollongong, hqmq581@uowmail.edu.au

Esraa Al-Shawwa
University of Science & Technology

Sameh Hamzawy
University of Wollongong, snsh769@uowmail.edu.au

Publication Details

AlZoubi, T., Qutaish, H., Al-Shawwa, E. & Hamzawy, S. (2018). Enhanced UV-light detection based on ZnO nanowires/graphene oxide hybrid using cost-effective low temperature hydrothermal process. Optical Materials, 77 226-232.

Enhanced UV-light detection based on ZnO nanowires/graphene oxide hybrid using cost-effective low temperature hydrothermal process

Abstract

A new low-cost optimized hydrothermal process of direct synthesis of ZnO nanowires (NWs)/graphene oxide (GO) hybrid on silicon substrates at a low growth temperature (~60°C) is reported. The careful optimization of the growth conditions and ZnO/GO relative ratios have resulted in high-density ZnO NWs formation with homogenous density and size distributions directly on GO sheets. The fabricated nanocomposites were intensively investigated by employing different structural, optical and electrical characterization techniques such as SEM, EDX, XRD, FTIR, UV-VIS and I-V. SEM analysis showed a formation of highly dense ZnO NWs on GO sheets with homogenous size di stributions with average approximate diameter and length of 70 nm and 310 nm, respectively. The EDX combined with FTIR and XRD measurements confirmed the exact chemical composition of the intended structure. The room-temperature UV-VIS spectra revealed an enhance optical absorption of UV-light at an absorption band centered at 370 nm. Under UV-excitation a significant photocurrent increase has been observed. This is can be attributed to the large surface to volume ratio in ZnO-NWs structure, which is associated with oxygen desorption at the large ZnO-NWs surfaces that reduces the recombination rate of photogenerated free charge carriers. The optimum electrical and optical properties of the device have been observed at ZnO-NWs/Go relative ratio of 1:5. These findings could be promising for potential enhanced UV-detectors and flexible optoelectronics devices.

Disciplines

Engineering | Physical Sciences and Mathematics

Publication Details

AlZoubi, T., Qutaish, H., Al-Shawwa, E. & Hamzawy, S. (2018). Enhanced UV-light detection based on ZnO nanowires/graphene oxide hybrid using cost-effective low temperature hydrothermal process. Optical Materials, 77 226-232.

Enhanced UV-light detection based on ZnO nanowires/graphene oxide hybrid using cost-effective low temperature hydrothermal process

Authors: Tariq AlZoubi[1], Hamzeh Qutaish[2], Esra'a Al-Shawwa[3], Sameh Hamzawy[2]

[1] College of Engineering and Technology, American University of the Middle East (AUM), P.O. Box 220 Dasman, 15453 Kuwait

[2] Australian Institute for Innovative Materials (AIIM), University of Wollongong (UOW), Squires Way, North Wollongong, NSW, 2500, Australia

[3] Department of Biomedical Engineering, Jordan University of Science & Technology (JUST), P.O. Box 3030, Irbid 22110, Jordan

Abstract:

A new low-cost optimized hydrothermal process of direct synthesis of ZnO nanowires (NWs)/ graphene oxide (GO) hybrid on silicon substrates at a low growth temperature ($\sim 60\,^{\circ}C$) is reported. The careful optimization of the growth conditions and ZnO/GO relative ratios have resulted in high-density ZnO NWs formation with homogenous density and size distributions directly on GO sheets. The fabricated nanocomposites were intensively investigated by employing different structural, optical and electrical characterization techniques such as SEM, EDX, XRD, FTIR, UV-VIS and I-V. SEM analysis showed a formation of highly dense ZnO NWs on GO sheets with homogenous size distributions with average approximate diameter and length of 70 nm and 310 nm, respectively. The EDX combined with FTIR and XRD measurements confirmed the exact chemical composition of the intended structure. The room-temperature UV-VIS spectra revealed an enhance optical absorption of UV-light at an absorption band centered at 370 nm. Under UV-excitation a significant photocurrent increase has been observed. This is can be attributed to the large surface to volume ratio in ZnO-NWs structure, which is associated with oxygen desorption at the large ZnO-NWs surfaces that reduces the recombination rate of photgenerated free charge carriers. The optimum electrical and optical properties of the device have been observed at ZnO-NWs/Go relative ratio of 1:5. These findings could be promising for potential enhanced UV-detectors and flexible optoelectronics devices.

1. Introduction

ZnO is described as a functional, strategic, promising, low cost, and versatile inorganic material with a wide range of applications. It is known as II–VI semiconductor, since Zn and O are classified into second and sixth groups of the periodic table, respectively [1]. ZnO possesses a unique optical, chemical sensing, semiconducting, electric conductivity, and piezoelectric properties [2]. It is characterized by a direct wide band gap (3.3 eV) in the near-UV spectrum with high exciton binding energy of (60 meV) at room temperature, which has a significant effect on its properties, such as the electrical conductivity and optical absorption [3-7]. These characteristics enable ZnO to have remarkable applications in diverse fields such as electronic and optoelectronic devices, chemical sensors, and biosensors [8-11]. Due to its superior optical properties, ZnO has been highly used in ultraviolet (UV) photodetectors. Moreover, ZnO-based UV-detectors have the advantage to be insensitive to the visible light allowing for visible-blind detection without any additional filters compared to other semiconductor materials, which are used for these applications [12-16].

Enhancing the collection of incident photons thereby the generated photocurrent are key parameters in today UV-photodetectors design and development. ZnO-nanowires (NWs) are highly preferable in this direction due to its large surface-to-volume ratio compared with other reported nanostructures [17-19]. However, further improvement of UV-photodetectors internal parameters such as sensitivity, responsivity, detectivity, photocurrent gain, rise time and decay time are still remained a challenge in modern flexible optoelectronics devices.

ZnO/carbon-based hybrid nanomaterials have attracted interest as a way to further improve the ZnO nanowires (NWs) based photodetectors performance [20-25]. Integration of graphene (G) into optoelectronic devices such as UV-light sensors have a strong impact on their performance and applications, due to it is high optical transmission property (97.7%), which in turns maximize the UV-light absorption in these devices [26-29]. In addition, graphene has a superior electrical conductivity, which can effectively prevent the recombination of the electron-hole pairs in the ZnO/G nanocomposites and thereby increase the photocurrent of the sensor for detection without requiring high-precision measurement [30-35]. Many methods have been employed for the synthesis of ZnO-NWs including Vapor liquid solid (VLS) growth [36], chemical vapor deposition (CVD) [37], metal organic chemical vapor deposition (MOCVD) [38], physical vapor deposition (PVD) [39], molecular beam epitaxy (MBE) [40], pulsed laser deposition (PLD) [41], and metal organic vapor phase epitaxy (MOVPE) [42]. However, all these methods are carried out at elevated growth temperatures (450 °C - 1500 °C) using very complex and expensive techniques. Further reduction in the growth temperature (< 80 °C) of ZnO-NWs based-devices can replace the expensive substrates by cheaper and more flexible substrates.

Therefore, photodetectors synthesized at reduced temperatures methods play a key role in cost reduction and open more choices of flexible substrates selection, which are highly desirable in flexible optoelectronics technology.

The hydrothermal process is one of the prime candidates that has attracted considerable attention due to its unique advantages such as simplicity, low cost, more controllable and low temperature (< 100 °C) compared with the previously discussed methods. Despite of these research efforts, few reports have studied ZnO-NWs /graphene oxide (GO) sheets system using hydrothermal process, which is likely due to the absence of effective morphological and interfacial control between ZnO nanostructures and graphene [43-46]. The motivation of this work is to take advantage of the superior optical properties of ZnO nanowires combined with the flexible, transparent and ideal transport properties of graphene into a single device. As a result, leading to a remarkable enhancement of photodetector internal parameters. However, excellent flexible UV-photodetectors can be used in wide range of applications such as automobiles, fire detection, environmental studies, pharmaceuticals, robotics, medical and communication equipment, biosensors, chemical industry for the production, storage of chemicals, and recently in space exploration [47, 48].

In this paper, we report on exploring high performance, large-scale, cost effective UV- sensor, which is highly compatible with flexible electronics. This UV-detector is synthesized by ZnO nanowires/GO sheets hybrid using a low temperature hydrothermal process directly on silicon substrate.

2. ZnO nanowires growth and UV detector design

2.1 Hydrothermal Synthesis of ZnO-Nanowires/GO sheets:

ZnO-NWs have been prepared by mixing ZnO-nanoparticles with a growth solution under a water path at a low temperature of (~ 60 °C). The detailed description of ZnO-NPs preparation has been already reported in our previous work [49]. The ZnO-nanoparticles serve as seeds and nucleation sites to initiate the growth of ZnO-NWs on GO sheets inside the growth solution. After preparing the zinc oxide nanoparticles, a solution of distilled water and graphene was sonicated for 30 min, then the ZnO-NPs solution was added to the graphene solution with different relative ratios (ZnO-NPs/GO) 1:25, 1:5, and 1:1, respectively. The used growth solution was prepared from 0.5488 g zinc acetate and 0.7437 g zinc nitrate in 100 ml of distilled water.

All n-type Si (100) substrates underwent a wet etching cleaning for oxides removal using HCL for 2 min. The nanocomposite mixtures solution prepared in the previous step was put on Si substrates and left to dry for 24 hours at room temperature. After that, the holder that holds

the silicon substrates was dunk in the growth solution in a water path at temperature of 60 C^{o} for 7 hours.

2.2 UV detector of ZnO-NWS/GO/Si design

The holder together with the surface treated Si-substrates that submersed in the growth solution in the last step were lifted from the growth solution. At the end, all samples were cleaned using DI water and left to dry at room temperature. After drying, a very thin layer of Ag was printed on the UV detector structure as shown in Fig. [1]. Subsequently, Cu electrodes were fixed over Ag contacts using heat and a duct tape.

3. Results and discussion

The successful formation of ZnO-NWs on GO sheets was evaluated using various structural, optical and electrical characterization tools. These investigations have been performed with the help of electron dispersive x-ray (EDX), scanning electron microscope (SEM), x-ray diffraction (XRD), Fourier transform infrared spectroscopy (FTIR), ultra violet-visible absorption spectroscopy (UV-VIS), and current-voltage (IV) measurements.

3.1 Structural and compositional characterizations

3.1.1 XRD studies

Fig. 2 shows the XRD measurement of ZnO-NWs/GO/Si composite. The typical Si substrate peak (100) reflection was observed with highest intensity at a diffraction angle 2θ of 26.7°. However, (002) GO reflection was detected at an angle 2θ of 12.71° with relatively lower intensity, this confirms the partial reduction of GO to graphene sheets. All ZnO major reflections are observed at 2θ = 31.81°, 34.6°, 36.4°, 47.7°, 54.9°, 56.7°, 63.3°, 68.1° and 69.2°, which correspond, respectively, to the (100), (002), (101), (110), (102), (103), (200),(112) and (201) planes of ZnO (Joint Committee on Powder Diffraction Standards 36-1451). All peaks in the ZnO-NWs can be indexed to hexagonal wurtzite structure with space group P63mc and lattice parameters a = 0.3251 nm and c= 0.5208 nm, which indicates that ZnO nanowires are oriented to some extent [50, 51]. No extra diffraction peaks of other phases have been detected, indicating the phase purity of the nanocomposite.

3.1.2 EDX for Chemical composition analysis

The chemical compositions of the ZnO-NWs/GO nanocomposite (sample with ratio 1:5) was characterized by a scanning electron microscope SEM equipped with an energy dispersive X-ray (EDX). EDX analysis of the chemical composition as-prepared ZnO-NWs/GO nanocomposite on

Si substrate shows that only Zn, O, C and Si substrate signals have been detected (Fig. 3), which indicate that the hybrid structure indeed made up of Zn, O, C and Si elements. No signal of secondary phase or impurity was detected, thus suggested the high-purity of the grown structure.

3.1.3 Morphological studies

SEM has been utilized for the purpose of morphological study of the grown ZnO/GO nanocomposites. Fig. [4] depicts the SEM images for different ZnO:GO relative ratios of 1:1, 1:5, and 1:25, respectively. A clear high dense ZnO-NWS with homogenous size and density is observed at relative ratio of 1:1 (Fig. 4-a).

Fig.4-b with a relative ratio of 1:5 shows less dense ZnO-NWs formation compared to 1:1 ratio. However, no ZnO-NWs has been observed at a relative ratio of 1:25 (Fig.4-c). This might be attributed as a formation of ZnO nanoparticles instead on nanowires with kind of aggregation behavior that tend to form bigger islands with random growth directions. One possible reason for that growth structure is the less ZnO concentration compared to GO, which is not sufficient to initiate the growth of ZnO-NWs that observed to form at higher ZnO concentrations.

3.1.4 FTIR spectroscopy

The surface modifications of the functional groups of ZnO-NWs/GO after the hydrothermal process have been investigated by FTIR spectroscopy. Fig. 5 shows FTIR spectrum of the absorption bands of ZnO-NWs/GO nanostructure with a relative concentration of 1:5.

All oxidized samples exhibit an absorption band centered at 442 cm^{-1}, related to the stretching mode of Zn-O bond vibration [1]. The peaks at 3451, 1740, 1683 and 724 cm^{-1} are assigned to O-H stretching vibration, C=O stretching, C=C bond stretch in alkenes and C-H rock, respectively [2-4]. The FTIR spectrum results are in a good agreement with ZnO-NWs/GO contents obtained by XRD and EDX analysis.

3.2 Optical characterization via UV-VIS

Fig. 6 shows the UV-VIS absorption spectra for a water solution of pure ZnO nanowires (ZnO-NWs) and ZnO-NPs, pure graphene oxide (GO), and ZnO-NWs/GO with different relative ratios 1:25, 1:5, and 1:1. The ZnO-NWs solution shows the characteristic UV sharp peak absorption centered at 370 nm (~ 3.35 eV) [50], which near to the energy gap of bulk ZnO, with an absorption of about 60 % of the incident UV-light. The peak found at about 260 nm, which is much below the energy gap of ZnO, is mostly because of the ZnO nanoparticles formation in this sample [51].

It can also be clearly seen that the UV light absorption with sharp peak cantered at 370 nm decreases with the decreasing of ZnO-NWs concentration in the solution. This explains that UV

absorption is directly associated with the ZnO concentration in the sample, which confirms that ZnO-NWs acts as UV absorbing and charge carriers generating material.

3.3 I-V characteristics of ZnO-NWs/GO/Si nanocomposite

A UV light source with a wavelength of 365 nm and power density of 10 mW/cm^2 at the bias of 6 V has been utilized for the I-V measurements with UV illumination. Fig. 7a shows different photoresponse log scale I-V curves under dark and UV conditions for two different relative ratios of ZnO-NWs/GO 1:1 and 1:5, respectively. All I-V curves look quiet symmetric for all samples, indicating good ohmic contacts on both sides. Under UV excitation a clear reasonable photocurrent increase for both samples has been observed. The sample with 1:5 relative ratio exhibited a higher photocurrent increase compared to the one with 1:1 relative ratio. This could be attributed to the increase of ZnO-NWs density, which form closer NWs structure in 1:1 sample. As a result, ZnO-NWs cover the entire graphene sheets and decrease the contacts between GO sheets themselves. This suggests the raise of the device resistivity and decrease in photocurrent compared to the sample with lower ZnO-NWs/GO ratio 1:5.

The difference in the current behavior upon UV irradiation could be explained as follows; in the darkness with complete absence of UV radiation, oxygen molecules are adsorbed by ZnO NWs surfaces directly from ambient air. Free electrons from n-type ZnO are trapped by oxygen molecules and form negative ions $-O_2$ on the surface of ZnO NWs. The oxygen adsorption process lowers the conductivity on the surface of ZnO NWs by forming a non-conducting depletion layer [51]. However, Under UV irradiation, electron-hole pairs are generated and negative oxygen ions ($-O_2$) capture the free holes, which neutralized the oxygen ions and activate the desorption of oxygen molecules from the ZnO-NWs surface. This suggests the rise of the amount of free charge carriers and lower the surface depletion thickness in NWs, which enhances the photoconductivity of the device [52].

The presence of graphene in contact with the metal electrodes improve the probability of conduction between the Ag electrode – graphene sheets by decreasing the electrical path of the photogenerated free charge carriers in the designed detector. In addition, the transferred photogenerated free charge carriers from ZnO-NWs to graphene is enhanced due to the high transport mobility of graphene [53]. This reduces the recombination rate of the photogenerated free charge carries and increase the photocurrent in the ZnO-NWs/GO device.

Fig. 7b depicts the influence of ZnO-NWs/GO/Si nanocomposite annealing on the I-V characteristics (sample with ratio 1:5). Under UV illumination, the obtained results show a slight photocurrent decrease in the sample annealed at 300 °C compared to the sample as grown and measured at room temperature. This suggests that the UV-photodetector is relatively thermally stable up to 300 °C. However, further annealing of ZnO-NWs (> 600 °C) has been proven to have a significant impact on ZnO-NWs diameters thus their density. ZnO-NWs diameters have been found to increase with the increase of annealing temperature above 600 °C [54-58]. Low density ZnO-NWs results in less photons harvesting due to the decrease of the ZnO-NWs total

surface area which is exposed to UV-radiation. Therefore, this results in less photocharge carrier generation, which degrade the overall UV-photodetector performance.

3.4 UV-Photodetector internal performance parameters analysis

In this study, the spectral responsivity (R_s) of ZnO-NWs/GO nanocomposite device has been calculated using eq. 1. Responsivity defined as the ratio of the photocurrent ($I_{Ph} = I_{UV} - I_{dark}$) to the incident excitation power density (P_{in}), where A is the effective device area of UV-illumination [59, 60].

$$R_s = \frac{I_{Ph}}{A\,P_{in}} \qquad (1)$$

Fig. 8a (circular dots line) shows the calculated responsivity of ZnO-NWs/GO device at different bias voltages ranging from 1 to 5 volts. Maximum responsivity of 10.13×10^3 A/W has been obtained for ZNO-NWs/GO nanostructure at applied bias voltage of 5 V. This corresponds to an enhancement factor of about 14 times higher than similar recently reported structures [63]. This enhancement is attributed to the enhanced mobility of the photgenerted carrier due to the presence of graphene sheets and the improved interfacial morphology and contacts between the nanocomposites in this device compared to other devices [64,65]. A comparison study between the results of the present work versus other reported photodetectors is summarized in Table. 1. Fig. 8a (square dots line) illustrates the calculated photocurrent gain (G) as a function of the bias voltage. Assuming that no optical losses and all photons are absorbed by the device, the gain can be calculated by applying eq. 2.

$$G = \frac{R_s}{q/h\nu} \qquad (2)$$

It can be observed from fig. 8a that responsivity and photocurrent gain vary almost linearly with the bias voltage due to the increased drift velocity of the charge carriers. The maximum photocurrent gain obtained as high as 3.45×10^4 at a bias voltage of 5 volts. The sensitivity, which is defined as the ratio of photocurrent to the dark current is about 1.7. This value is comparable with the recent excellent reported photodetectors that are synthesized via expensive and complex techniques [45, 46, 65].

Fig. 8b displays the time-dependent response photocurrent in GO/ZnO-NWs device for 3 min UV exposure at a bias voltage of 5 V. A sudden rise in photocurrent has been observed that quickly reaches its maximum value. This can be characterized by the rise time (τ_r), which is defined as the time needed to reach 90 % of the maximum current. Whereas the decay time (τ_d) defined as the time needed to drop to 10 % from the maximum current. Fig. 8b reveals a fast rise and decay times of about 11.2 s and 81 s, respectively. This relatively fast response performance is in a good agreement to the previous reported experimental results (see table 1). The outcomes of the prepared ZnO-NWs/GO photoconductor analysis exhibits a very good

optoelectronics properties. These findings could be promising for potential enhanced UV-detectors and flexible optoelectronics devices.

4. Conclusion

High-dense ZnO nanowires have been successfully grown directly on graphene oxide sheets by simple cost-effective and low temperature hydrothermal method. EDX, XRD, FTIR measurements of the fabricated ZnO-NWs/GO nanocomposites confirmed the exact chemical compositions of the intended structure with high purity. All samples of ZnO-NWs/GO with various relative ratios of 1:1, 1:5, and 1:25 exhibited UV light absorption at a band centered at 370 nm. The absorbed UV light has been observed to increase with the increase of the ZnO-NWs concentration in the samples. The photocurrent under UV irradiation was considerably enhanced compared in the dark conditions. This enhancement is attributed to the adsorbed oxygen on ZnO-NWs surface and the photogenerated holes, which ultimately can neutralize the oxygen. As a result, this can promote spatial separation of electrons and photogenerated holes, thereby decreasing their recombination rate. In addition, to the enhanced transport mobility in the presence of graphene, which increases the recombination life time of the photogenerated carriers and thereby increase the photocurrent in ZnO-NWs/GO based devices.

Acknowledgments

We gratefully thank the financial and technical support provided by the institute of nanotechnology at the Jordan University of Science and Technology.

Figure Captions:

Fig. 1: Schematic of UV-photodetector based on ZnO-NWs/Go/Si hybrid structure.

Fig. 2: XRD of ZnO-NWs/GO nanocomposite on Si substrate sample with relative ratio of 1:5.

Fig. 3: EDX measurement of ZnO-NWs/GO/Si with relative ratio 1:5. The inset shows SEM image of the same with high density ZnO-NWs on graphene sheets.

Fig. 4: SEM images of ZnO-NWs/GO nanocomposites on Si substrate with different relative ratios. (a) 1:1, (b) 1:5 and (c) 1:25, respectively.

Fig. 5: FTIR spectrum of ZnO-NWs/graphene nanocomposite with 1:5 relative ratios.

Fig. 6: UV-VIS absorption spectra of zinc oxide nanowires ZnO-NWs and some ZnO nanoparticles (pink), graphene oxide (GO) (black), and ZnO-NWs/GO ratios of 1:1 (blue), 1:5 (amber), and 1:25 (red). All solutions were in water.

Fig. 7: (a) Current – Voltage (I-V) characteristics of ZnO-NWs/GO nanocomposite: (Black) I-V curve in dark, (blue) I-V curve under UV illumination for the sample with ratio 1:1. (red) I-V curve under UV illumination for the sample with ratio 1:5. (b) Current – Voltage (I-V) characteristics of ZnO-NWs/GO nanocomposite: (Black) I-V curve in dark, (red) I-V curve under UV illumination at 300 °C, (blue) I-V curve under UV illumination at 25 °C.

Fig. 8: (a) ZnO-NWs/GO spectral responsivity and photocurrent gain as a function of bias voltage. (b) Time-dependent photoresponse current of ZnO-NWs/GO hybrid under UV-illumination and dark conditions at 5 V bias.

Table caption:

Table. 1: Responsivity and time-dependent photocurrent response comparison between the present work and similar reported UV-photodetectors structures.

UV-Sensor Structure	Rise Time (s)	Decay Time (s)	λ (nm)	Bais (V)	R_s (A/W)	Ref.
ZnO Nanorods/Graphene	n/a	n/a	370	20	22.7	[43]
ZnO NWs/Graphene foam	9.5	38	365	5	6	[44]
ZnO Nanorods	3.7	63.6	325	n/a	n/a	[61]
ZnO NWs	2	100	360	1	39	[62]
ZnO NWs/G	269	139	352	3	728	[63]
ZnO NWs	229	547	310	3	n/a	[65]
Graphene/ZnO NWs	11.9	240	365	5	32000	[45]
Graphene/ZnO NW/Graph	3	0.47	365	5	23	[46]
ZnO NWs/Graphene	11.2	81	370	5	10230	This work

References:

1. Neumark, G., Y. Gong, and I. Kuskovsky, *Doping Aspects of Zn-Based Wide-Band-Gap Semiconductors*, in *Springer Handbook of Electronic and Photonic Materials*. 2006, Springer. p. 843-854.

2. Fan, Z. and J.G. Lu, *Zinc oxide nanostructures: synthesis and properties.* Journal of nanoscience and nanotechnology, 2005. **5**(10): p. 1561-1573.

3. Schmidt-Mende, L. and J.L. MacManus-Driscoll, *ZnO–nanostructures, defects, and devices.* Materials today, 2007. **10**(5): p. 40-48.

4. Wang, Z.L., *Zinc oxide nanostructures: growth, properties and applications.* Journal of Physics: Condensed Matter, 2004. **16**(25): p. R829.

5. Wang, Z.L. and J. Song, *Piezoelectric nanogenerators based on zinc oxide nanowire arrays.* Science, 2006. **312**(5771): p. 242-246.

6. Wellings, J., et al., *Growth and characterisation of electrodeposited ZnO thin films.* Thin solid films, 2008. **516**(12): p. 3893-3898.

7. Zhang, Y., et al., *Synthesis, characterization, and applications of ZnO nanowires.* Journal of Nanomaterials, **2012**: p. 20.

8. Boruah, B.D., et al., *Highly dense ZnO nanowires grown on graphene foam for ultraviolet photodetection.* ACS applied materials & interfaces, 2015. **7**(19): p. 10606-10611.

9. Djurišić, A., A. Ng, and X. Chen, *ZnO nanostructures for optoelectronics: material properties and device applications.* Progress in Quantum Electronics, 2010. **34**(4): p. 191-259.

10. Kumar, N., A. Dorfman, and J.-i. Hahm, *Ultrasensitive DNA sequence detection using nanoscale ZnO sensor arrays.* Nanotechnology, 2006. **17**(12): p. 2875.

11. Umar, A., et al., *Zinc oxide nanonail based chemical sensor for hydrazine detection.* Chemical Communications, 2008(2): p. 166-168.

12. Peng, W., et al., *Performance improvement of ZnO nanowire based surface acoustic wave ultraviolet detector via poly (3, 4-ethylenedioxythiophene) surface coating.* Sensors and Actuators A: Physical, 2013. **199**: p. 149-155.

13. Duan, L., et al., *Fabrication of Self-Powered Fast-Response Ultraviolet Photodetectors Based on Graphene/ZnO: Al Nanorod-Array-Film Structure with Stable Schottky Barrier.* ACS Applied Materials & Interfaces, 2017. **9**(9): p. 8161-8168.

14. Liu, S., et al., *Enhanced sensitivity and response speed of graphene oxide/ZnO nanorods photodetector fabricated by introducing graphene oxide in seed layer.* Journal of Materials Science: Materials in Electronics, 2017: p. 1-8.

15. Basu, S. and A. Dutta, *Modified heterojunction based on zinc oxide thin film for hydrogen gas-sensor application.* Sensors and Actuators B: Chemical, 1994. **22**(2): p. 83-87.

16. Huang, M.H., et al., *Room-temperature ultraviolet nanowire nanolasers.* science, 2001. **292**(5523): p. 1897-1899.

17. Razeghi, M. and A. Rogalski, *Semiconductor ultraviolet detectors.* Journal of Applied Physics, 1996. **79**(10): p. 7433-7473.

18. Wan, Q., et al., *Fabrication and ethanol sensing characteristics of ZnO nanowire gas sensors.* Applied Physics Letters, 2004. **84**(18): p. 3654-3656.

19. Liu, K., M. Sakurai, and M. Aono, *ZnO-based ultraviolet photodetectors.* Sensors, 2010. **10**(9): p. 8604-8634.

20. Kind, H., et al., *Nanowire ultraviolet photodetectors and optical switches.* Advanced materials, 2002. **14**(2): p. 158.

21. Lupan, O., et al., *Well-aligned arrays of vertically oriented ZnO nanowires electrodeposited on ITO-coated glass and their integration in dye sensitized solar cells.* Journal of Photochemistry and Photobiology A: Chemistry, 2010. **211**(1): p. 65-73.

22. Swanwick, M.E., et al., *Near-ultraviolet zinc oxide nanowire sensor using low temperature hydrothermal growth.* Nanotechnology, 2012. **23**(34): p. 344009.

23. Huang, X., et al., *Graphene-based composites.* Chemical Society Reviews, 2012. **41**(2): p. 666-686.

24. Huang, X., et al., *Graphene-based materials: synthesis, characterization, properties, and applications.* small, 2011. **7**(14): p. 1876-1902.

25. Jiang, H., *Chemical preparation of graphene-based nanomaterials and their applications in chemical and biological sensors.* Small, 2011. **7**(17): p. 2413-2427.

26. Novoselov, K., et al., *Two-dimensional atomic crystals.* Proceedings of the National Academy of Sciences of the United States of America, 2005. **102**(30): p. 10451-10453.

27. Zhu, Y., et al., *Graphene and graphene oxide: synthesis, properties, and applications.* Advanced materials, 2010. **22**(35): p. 3906-3924.

28. Liu, Z., et al., *Nonlinear optical properties of graphene oxide in nanosecond and picosecond regimes.* Applied physics letters, 2009. **94**(2): p. 021902.

29. Wang, X., L. Zhi, and K. Müllen, *Transparent, conductive graphene electrodes for dye-sensitized solar cells.* Nano letters, 2008. **8**(1): p. 323-327.

30. Eda, G., G. Fanchini, and M. Chhowalla, *Large-area ultrathin films of reduced graphene oxide as a transparent and flexible electronic material.* Nature nanotechnology, 2008. **3**(5): p. 270-274.

31. Shen, L., et al., *Electron transport properties of atomic carbon nanowires between graphene electrodes.* Journal of the American Chemical Society, 2010. **132**(33): p. 11481-11486.

32. Gong, M., et al., *All-Printable ZnO Quantum Dots/Graphene van der Waals Heterostructures for Ultrasensitive Detection of Ultraviolet Light.* ACS nano, 2017. **11**(4): p. 4114-4123.

33. Han, S.T., et al., *An Overview of the Development of Flexible Sensors.* Advanced Materials, 2017.

34. Vessalli, B.A., et al., *ZnO nanorods/graphene oxide sheets prepared by chemical bath deposition for volatile organic compounds detection.* Journal of Alloys and Compounds, 2017. **696**: p. 996-1003.

35. Zare, M., et al., *Graphene oxide incorporated ZnO nanostructures as a powerful ultraviolet composite detector.* Journal of Materials Science: Materials in Electronics, 2017. **28**(9): p. 6919-6927.

36. Petersen, E.W., et al., Growth of ZnO nanowires catalyzed by size-dependent melting of Au nanoparticles. Nanotechnology, 2009. 20(40): p. 405603.

37. Protasova, L., et al., ZnO based nanowires grown by chemical vapour deposition for selective hydrogenation of acetylene alcohols. Catalysis Science & Technology, 2011. 1(5): p. 768-777.

38. Ashraf, S., et al., MOCVD of vertically aligned ZnO nanowires using bidentate ether adducts of dimethylzinc. Chemical Vapor Deposition, 2011. 17(1-3): p. 45-53.

39. Wang, L., et al., Synthesis of well-aligned ZnO nanowires by simple physical vapor deposition on c-oriented ZnO thin films without catalysts or additives. Applied Physics Letters, 2005. 86(2): p. 024108.

40 Wang, J., et al., Catalyst-free highly vertically aligned ZnO nanoneedle arrays grown by plasma-assisted molecular beam epitaxy. Applied Physics A, 2009. 97(3): p. 553.

41. Tien, L., et al., Synthesis and microstructure of vertically aligned ZnO nanowires grown by high-pressure-assisted pulsed-laser deposition. Journal of Materials Science, 2008. 43(21): p. 6925-6932.

42. Kitamura, K., et al., Fabrication of vertically aligned ultrafine ZnO nanorods using metal–organic vapor phase epitaxy with a two-temperature growth method. Nanotechnology, 2008. 19(17): p. 175305.

43. Wang, Z.L., *Ten years' venturing in ZnO nanostructures: from discovery to scientific understanding and to technology applications.* Chinese Science Bulletin, 2009. **54**(22): p. 4021-4034.

44. Boruah, B.D., et al., *Highly dense ZnO nanowires grown on graphene foam for ultraviolet photodetection.* ACS applied materials & interfaces, 2015. **7**(19): p. 10606-10611.

45. Boruah, B.D., et al., *Few-layer graphene/ZnO nanowires based high performance UV photodetector.* Nanotechnology, 2015. **26**(23): p. 235703.

46. Boruah, B.D., A. Mukherjee, and A. Misra, *Sandwiched assembly of ZnO nanowires between graphene layers for a self-powered and fast responsive ultraviolet photodetector.* Nanotechnology, 2016. **27**(9): p. 095205.

47. E. Muñoz, E. Monroy, J. Pau, F. Calle, F. Omnès and P. Gibart, "III nitrides and UV detection", *Journal of Physics: Condensed Matter*, vol. 13, no. 32, pp. 7115-7137, 2001.

48. D. Kim, B. Jung, Y. Kwon and H. Cho, "Highly Sensible ZnO Nanowire Ultraviolet Photodetectors Based on Mechanical Schottky Contact", *Journal of The Electrochemical Society*, vol. 159, no. 1, p. K10, 2012.

49. Al-Fandi, M., et al. *A prototype Ultraviolet Light Sensor based on ZnO Nanoparticles/Graphene Oxide Nanocomposite Using Low Temperature Hydrothermal Method*. in *IOP Conference Series: Materials Science and Engineering*. 2015. IOP Publishing.

50. Greene, L.E., et al., *Solution-grown zinc oxide nanowires.* Inorganic chemistry, 2006. **45**(19): p. 7535-7543.

51. Talam, S., S.R. Karumuri, and N. Gunnam, *Synthesis, characterization, and spectroscopic properties of ZnO nanoparticles.* ISRN Nanotechnology, 2012. **2012**.

52. Cammi, D. and C. Ronning, *Persistent photoconductivity in ZnO nanowires in different atmospheres.* Advances in Condensed Matter Physics, 2014. **2014**.

53. Bao, J., et al., *Photoinduced oxygen release and persistent photoconductivity in ZnO nanowires.* Nanoscale research letters, 2011. **6**(1): p. 404.

54. Hwang, J.O., et al., Vertical ZnO nanowires/graphene hybrids for transparent and flexible field emission. Journal of Materials Chemistry, 2011. 21(10): p. 3432-3437.

55. Park, H., et al., Graphene cathode-based ZnO nanowire hybrid solar cells. Nano letters, 2012. 13(1): p. 233-239.

56. Akhavan, O., Graphene nanomesh by ZnO nanorod photocatalysts. ACS nano, 2010. 4(7): p. 4174-4180.

57. Alver, U., et al., Optical and structural properties of ZnO nanorods grown on graphene oxide and reduced graphene oxide film by hydrothermal method. Applied Surface Science, 2012. 258(7): p. 3109-3114.

58. Soci C, Zhang A, Xiang B, Dayeh S A, Aplin D P R, Park J, Bao X Y, Lo Y H and Wang D 2007 *Nano Lett.* **7** 1003–9

59. J. Law and J. Thong, "Simple fabrication of a ZnO nanowire photodetector with a fast photoresponse time", *Applied Physics Letters*, vol. 88, no. 13, p. 133114, 2006.
54. Zhang, Y., et al., Synthesis, characterization, and applications of ZnO nanowires. Journal of Nanomaterials, 2012. 2012: p. 20.

60. Chang, Haixin, et al. "A highly sensitive ultraviolet sensor based on a facile in situ solution-grown ZnO nanorod/graphene heterostructure." *Nanoscale* 3.1 (2011): 258-264.

61. Ahn, S.E., et al., Photoresponse of sol-gel-synthesized ZnO nanorods. Applied Physics Letters, 2004. **84**(24): p. 5022-5024.

62. Weng, W., et al., A lateral ZnO nanowire photodetector prepared on glass substrate. Journal of The Electrochemical Society, 2010. **157**(2): p. K30-K33.

63. B. Cook, Q. Liu, J. Liu, M. Gong, D. Ewing, M. Casper, A. Stramel and J. Wu, "Facile zinc oxide nanowire growth on graphene via a hydrothermal floating method: towards Debye length radius nanowires for ultraviolet photodetection", J. Mater. Chem. C, vol. 5, no. 38, pp. 10087-10093, 2017.

64. Kar, J., et al., Fabrication of UV detectors based on ZnO nanowires using silicon microchannel. Journal of Crystal Growth, 2009. **311**(12): p. 3305-3309.

65. Bera, A. and D. Basak, Photoluminescence and photoconductivity of ZnS-coated ZnO nanowires. ACS applied materials & interfaces, 2010. **2**(2): p. 408-412.

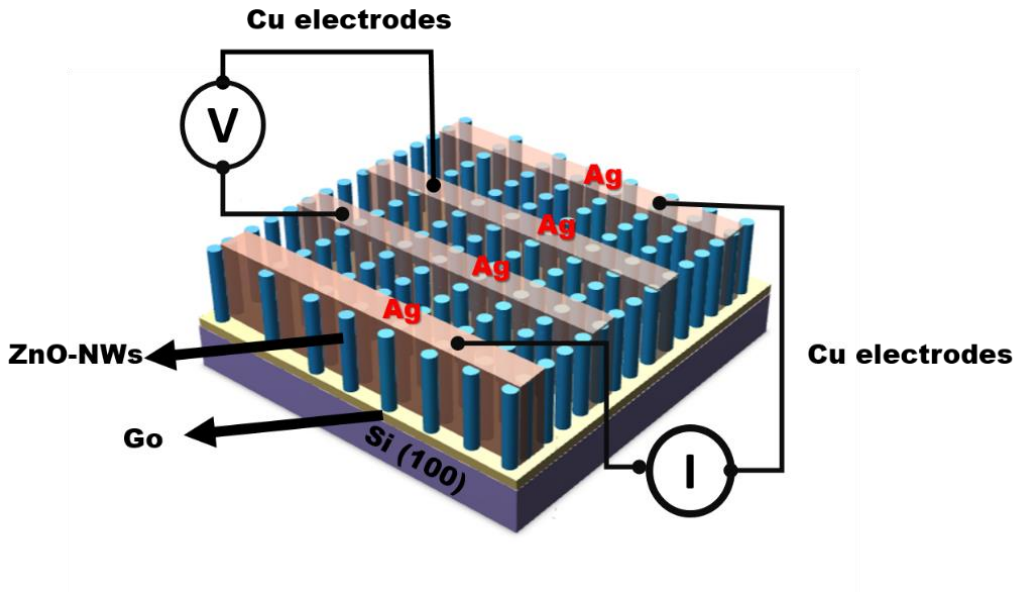

Figure (1)

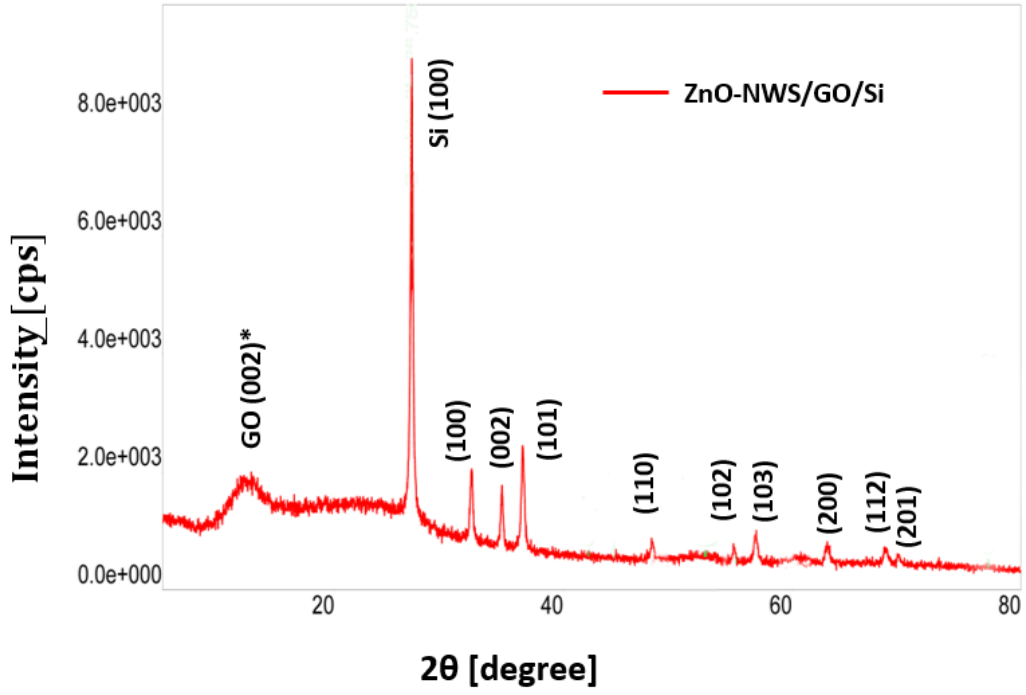

Figure (2)

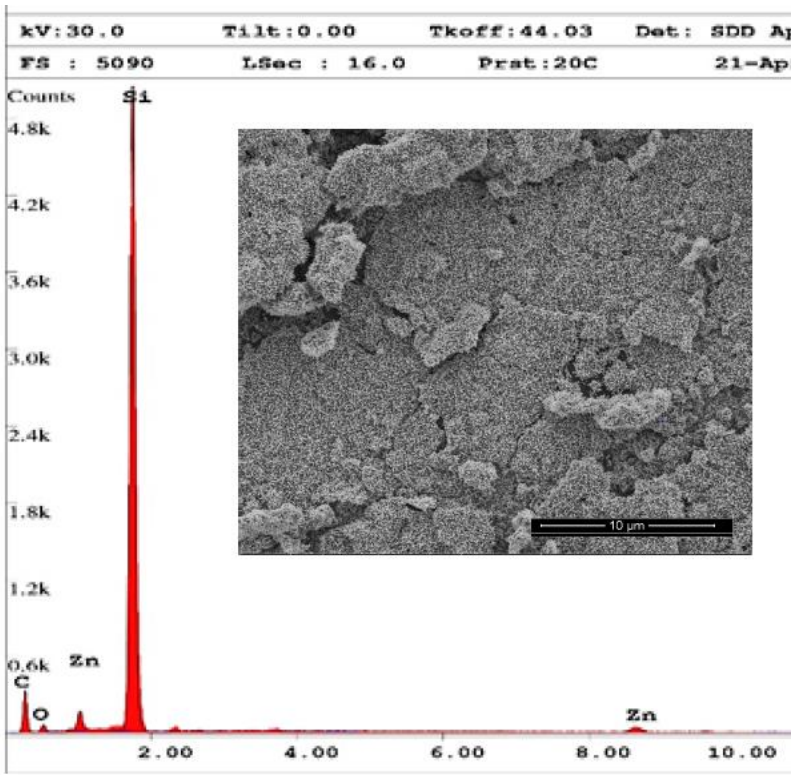

Figure (3)

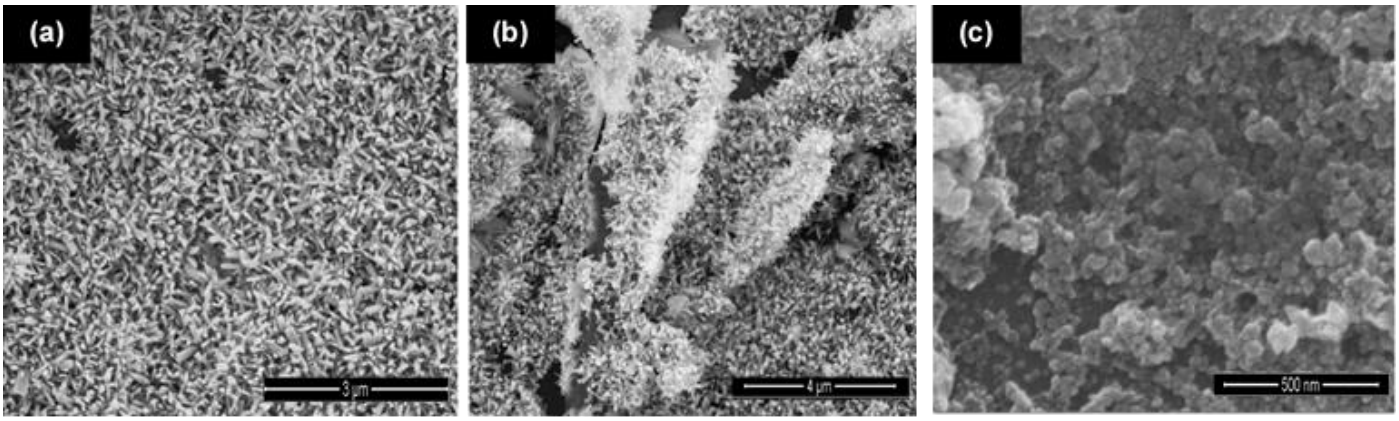

Figure (4)

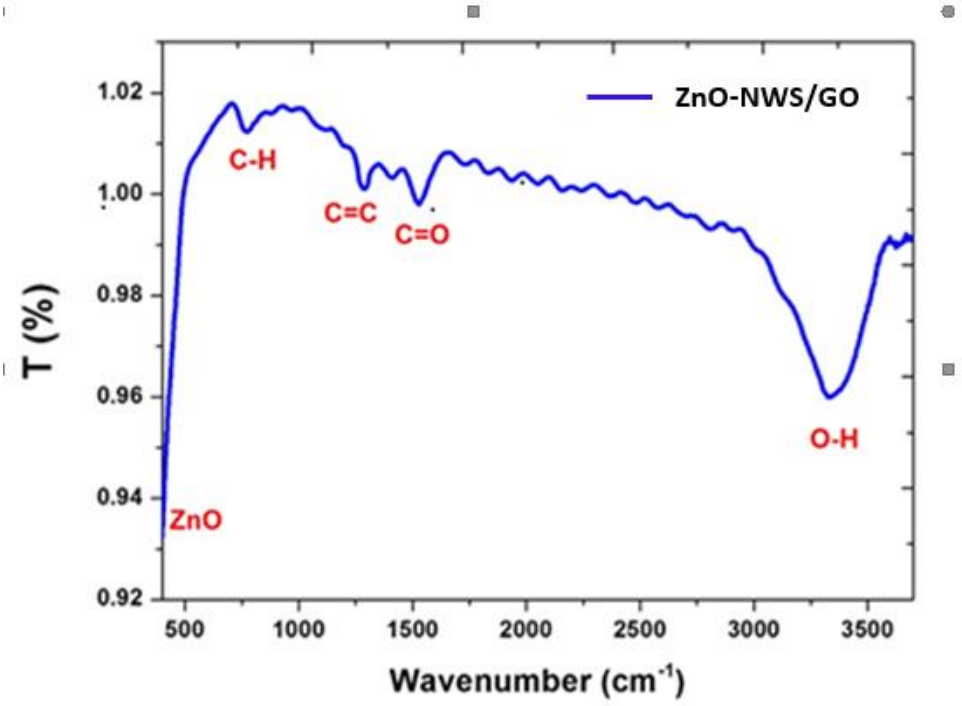

Figure (5)

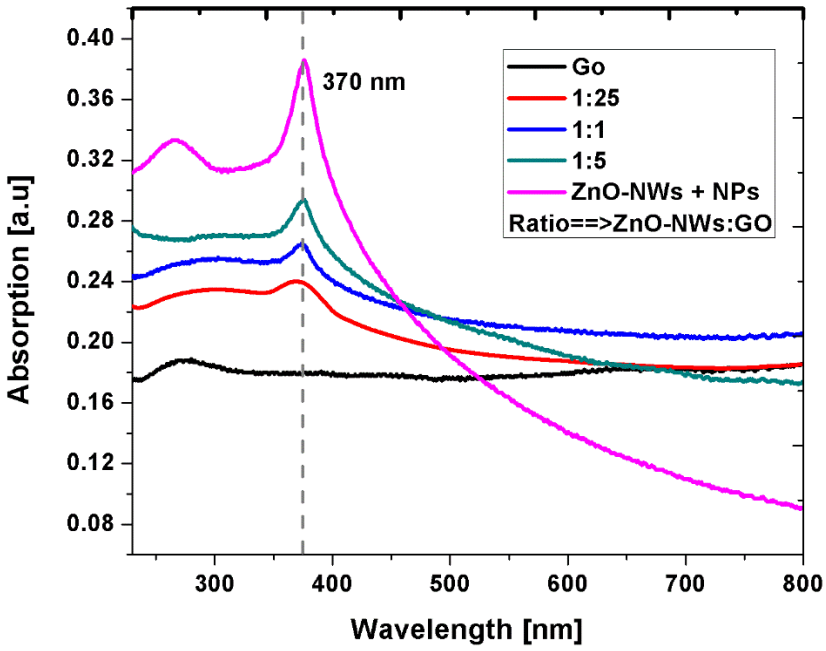

Figure (6)

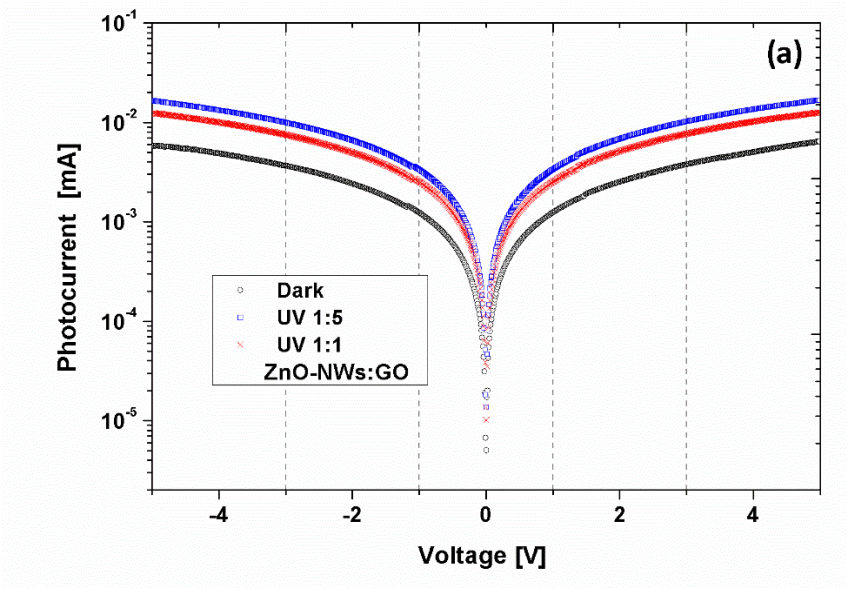

Figure (7a)

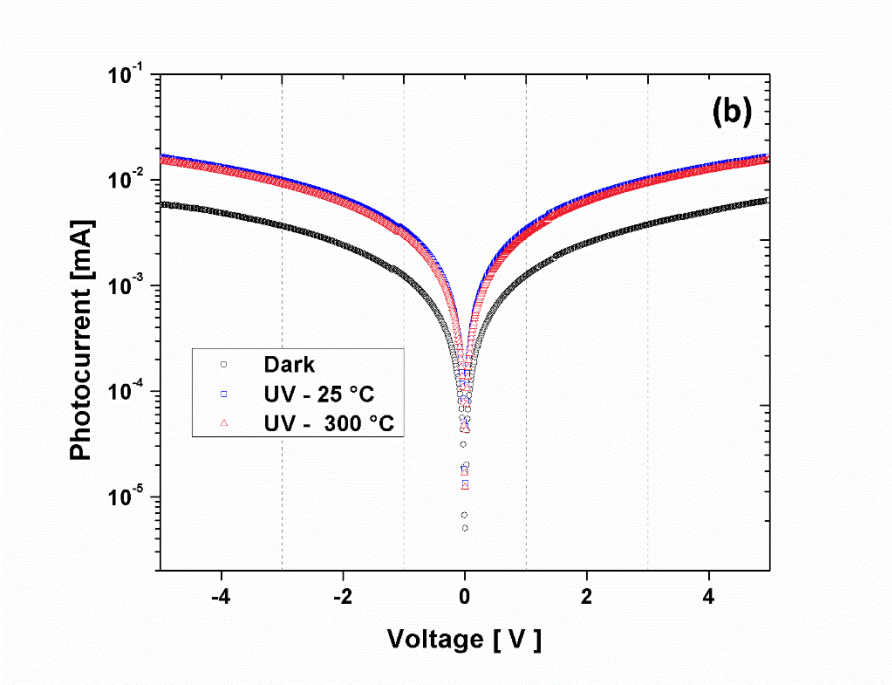

Figure (7b)

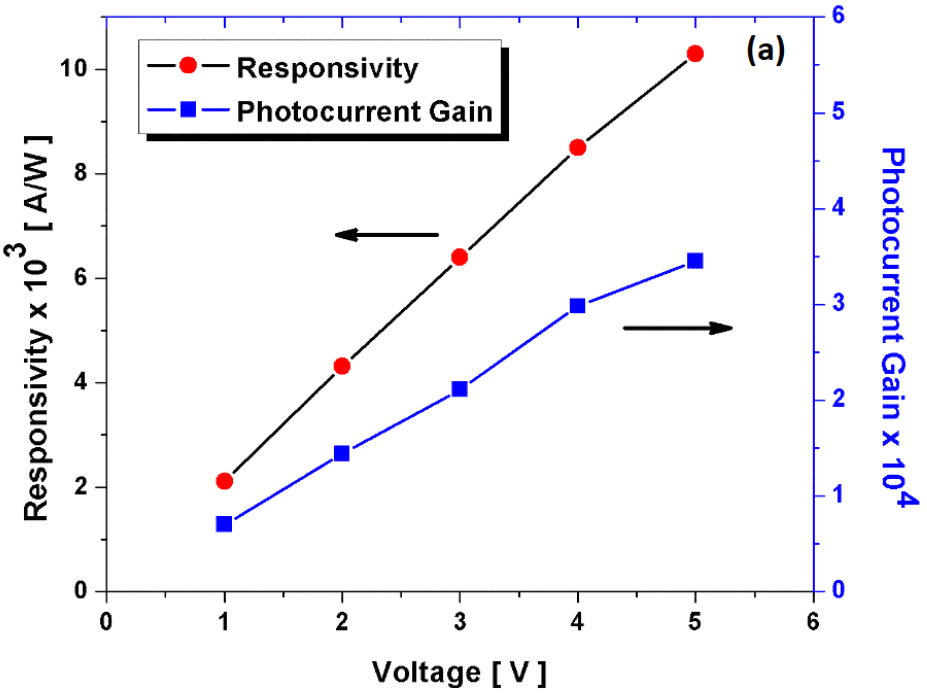

Figure (8a)

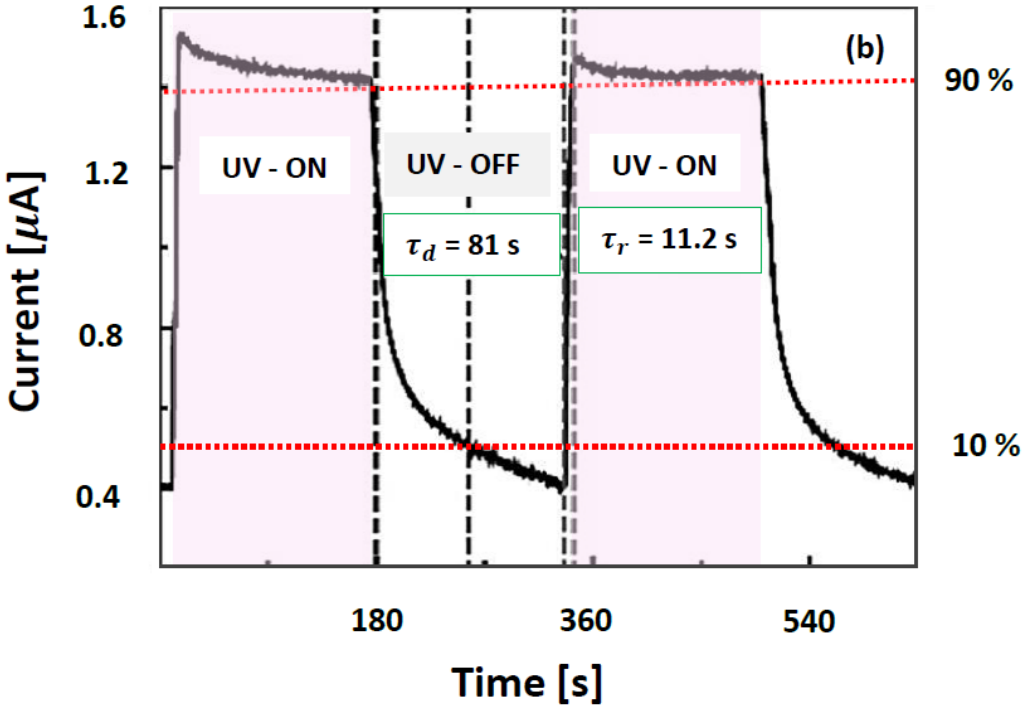

Figure (8b)